Published in final edited form as:
Thromb Res. 2012 September ; 130(3): e139–e146. doi:10.1016/j.thromres.2012.04.009.

Remodeling of Intramural Thrombus and Collagen in an Ang-II Infusion ApoE−/− Model of Dissecting Aortic Aneurysms

A.J. Schriefl[1], **M.J. Collins**[2], **D.M. Pierce**[1], **G.A. Holzapfel**[1,3], **L.E. Niklason**[4,5,6], and **J.D. Humphrey**[5,6]

[1]Institute of Biomechanics, Center of Biomedical Engineering, Graz University of Technology, Graz, Austria

[2]Department of Biomedical Engineering, Texas A&M University, College Station, TX, USA

[3]Department of Solid Mechanics, School of Engineering Sciences, KTH, Stockholm, Sweden

[4]Department of Anesthesiology, Yale School of Medicine, New Haven, CT USA

[5]Vascular Biology and Therapeutic Program, Yale School of Medicine, New Haven, CT USA

[6]Department of Biomedical Engineering, Yale University, New Haven, CT, USA

Abstract

Fibrillar collagen endows the normal aortic wall with significant stiffness and strength and similarly plays important roles in many disease processes. For example, because of the marked loss of elastic fibers and functional smooth cells in aortic aneurysms, collagen plays a particularly important role in controlling the dilatation of these lesions and governing their rupture potential. Recent findings suggest further that collagen remodeling may also be fundamental to the intramural healing of arterial or aneurysmal dissections. To explore this possibility further, we identified and correlated regions of intramural thrombus and newly synthesized fibrillar collagen in a well-established mouse model of dissecting aortic aneurysms. Our findings suggest that intramural thrombus that is isolated from free-flowing blood creates a permissive environment for the synthesis of fibrillar collagen that, albeit initially less dense and organized, could protect that region of the dissected wall from subsequent expansion of the dissection or rupture. Moreover, alpha-smooth muscle actin positive cells appeared to be responsible for the newly produced collagen, which co-localized with significant production of glycosaminoglycans.

Keywords

thrombosis; glycosaminoglycans; collagen remodeling; rupture; thoracic aneurysm

INTRODUCTION

Thoracic aortic aneurysms (TAAs) and abdominal aortic aneurysms (AAAs) are responsible for significant morbidity and mortality, with younger individuals (< 60 years old) affected

Address for Correspondence: J.D. Humphrey, Ph.D., Department of Biomedical Engineering, Malone Engineering Center, Yale University, New Haven, CT 06520–8260, (P) +1–203–432–6428, (F) +1–203–432–0030, jay.humphrey@yale.edu.

more by the former and older individuals (>70 years old) increasingly affected more by the latter in our aging society. Despite differences in etiology and natural history, fundamental mechanisms are shared by these two classes of lesions, including loss of elastin, apoptosis of smooth muscle, and remodeling of collagen (Sakalihasan et al., 2005; Milewicz et al., 2008). There is a continuing need, however, for an increased understanding of the biochemomechanical conditions that lead to dilatation, dissection, and rupture (Vorp, 2007; Humphrey and Taylor, 2008; Humphrey and Holzapfel, 2012). Motivated largely by the difficulty of collecting sufficient longitudinal information on lesion morphology, histology, cell biology, and biomechanical properties in humans, various animal models have been developed to study aortic aneurysms (cf. Daughtery and Cassis, 2004). Of the different models, continuous subcutaneous infusion of angiotensin-II (Ang-II) in the apolipoprotein-E null (ApoE−/−) mouse has emerged as the most commonly used method to generate dissecting aortic aneurysms (e.g., Saraff et al., 2003; Barisione et al., 2006; Satoh et al., 2008; Cassis et al., 2009; Rush et al., 2009; Cao et al., 2010; Goergen et al., 2011; Rateri et al., 2011; Trachet et al., 2011). Via these and many similar studies, it appears that these lesions initiate following an accumulation of macrophages within the media, which produce cytokines and proteases that lead to degradation, dissection, and dilatation of the wall. Hence, although these lesions occur primarily in the suprarenal abdominal aorta, they exhibit some features (e.g., dissection and intramural thrombus) that are more common to TAAs than to AAAs in humans. Regardless of localization, for the purposes herein, lesions arising from the infusion of Ang-II in ApoE−/− mice provide an excellent model of a dissecting aortic aneurysm, including development of an intramural thrombus and possible subsequent healing of the dissected wall.

Not with standing the availability of significant information on the histology and cell biology associated with the Ang-II mouse model of dissecting aneurysms (cf. Daugherty et al., 2011 and references therein), little attention has been directed towards the turnover of fibrillar collagens and possible roles played therein by intramural or intraluminal thrombus. Because of the marked loss of elastic fibers and functional smooth muscle cells within the aneurysmal wall, fibrillar collagens play particularly important mechanical roles in controlling the rate of enlargement and governing the rupture-potential (Humphrey and Holzapfel, 2012). In particular, given that collagen is very stiff when straight (with an elastic modulus on the order of 1 GPa), vascular distensibility depends largely on the degree of undulation of the collagen fibers as well as on their density, fiber diameter, interactions with other matrix proteins and glycoproteins, and cross-linking (Humphrey, 2002). In this paper, we examine for the first time the waviness and density of fibrillar collagens at different locations within serial cross-sections along the length of dissecting aortic aneurysms that developed due to a 28-day infusion of Ang-II, with particular attention to the replacement of intramural thrombus with fibrillar collagen during this period.

METHODS

Animal Model

All animal protocols were approved by the Texas A&M University Institutional Animal Care and Use Committee. Following other reports (e.g., Barisione et al., 2006), 8-week old male ApoE−/− mice were anesthetized with isoflurane and implanted subcutaneously in the mid-scapular region with an Alzet mini-osmotic pump (Durect Corp., CA). These pumps delivered Ang-II continuously at 1000 ng/kg/min. Following 28 days of treatment with Ang-II, while maintained on a normal diet, the mice were euthanized with an overdose of sodium pentobarbital. The suprarenal aorta was then isolated via a mid-line incision and photographed, large branches were ligated with 7-O silk, and the vessel was excised en-bloc. Following biomechanical testing (Genovese et al., 2012), the vessels were fixed in an unloaded configuration using a buffered 10% formalin.

Histology

Suprarenal aortas from five, 12-week old mice that developed significant aneurysms (> 1.5 fold increase in outer diameter) were cut into distal and proximal halves, embedded in paraffin (both halves in one block), and sectioned at five microns. Serial cross-sections were obtained for each half of the specimen at three axial locations separated by 880 microns, hence yielding 6 sets of axially located cross-sections per lesion. Supplemental Figure 1 gives an overview of the many resulting cross-sections for each vessel and thus illustrates the sectioning protocol. Sections were then stained with Verhoeff Van Gieson (VVG) to highlight elastin, picrosirius red (PSR) to highlight fibrillar collagens, Alcian blue to highlight glycosaminoglycans (GAGs), and Movat's pentachrome to identify fibrin, elastin, collagen, and glycosaminoglycans within a single section. Additional sections were immunostained for α-smooth muscle actin (αSMA). All images were acquired with an Olympus BX51TF microscope using an Olympus DP70 camera in combination with Olympus CellSens Dimension 1.4.1 software. In the case of the PSR-stained sections, images were acquired using appropriate polarizing optics and dark-field imaging; all other images were acquired using bright-field imaging. Magnification was typically set at 10X or 20X.

Image Analysis

As a measure of collagen waviness, we computed the "entropy" H from dark-field PSR-stained images collected from multiple locations within each cross-section. Straighter (more organized) fibers yield lower values of entropy whereas increasingly wavy (more disorganized) fibers yield higher values of entropy. Toward this end, each original dark-field image was first converted to an 8-bit (0 – 255) grayscale image that was then partitioned into five smaller images at each location to define multiple computational sub-domains for each calculation of waviness (Figure 1a). Each sub-domain was then divided into 25 × 25 pixel regions of interest (ROI), thus yielding n ROIs at each location of interest (cf. Figure 1b). The collagen fiber organization within each ROI was then represented by a distribution function $f(x,y)$, where (x,y) defines each point p in a 2-D real space. This distribution function was then transformed to the Fourier space using a 2-D fast Fourier transformation, which yielded $\Im(f(x,y)) = F(u,v)$, where (u,v) is the associated point in Fourier space. The zero-frequency components were then shifted to the center and, finally, the 2-D power spectrum P of the Fourier transform (FT) was obtained by multiplying the FT with its complex conjugate*, namely

$$P(u,v)=F(u,v)\cdot F^{*}(u,v). \quad (1)$$

The overall collagen fiber orientation within each ROI was then obtained by fitting a line through the center of the power spectrum in a least square sense (Xia and Elder, 2001). The orientation of the line yields the angle α as a measure of the overall fiber orientation for each ROI. All angles were then plotted as a histogram to yield a probability mass function $p(\alpha_i)$, which was normalized to $\sum_{i=1}^{n} p(\alpha_i)=1$ (Figure 1c). Finally, the entropy H was calculated from the probability mass function to yield a scalar measure of waviness of the collagen fibers, that is,

$$H=-\sum_{i=1}^{n} p(\alpha_i)\log_2 p(\alpha_i), \quad (2)$$

with n denoting the number of ROIs for each location of interest (Bayan et al., 2009).

To quantify the local density (or, "concentration") of the fibrillar collagen, we determined the area fraction of collagen present at multiple locations within each dark-field image. This quantification was performed on the same five computational sub-domains per location that were used to quantify waviness (cf. Figure 1a). This concentration was determined by calculating the ratio of colored pixels (representing the birefringent collagen fibers) to the black background for each domain. We emphasize that the term "concentration" is used loosely as a synonym for area fraction within a 2-D image and, therefore, should not be confused with the biochemical term concentration, as, for example, dry weight of collagen. All image analyses were performed using custom codes written in Matlab (MathWorks Inc., MA, USA). For isolating colors and applying color thresholds, we used ImageJ (U.S. National Institutes of Health, MD, USA).

RESULTS

Consistent with prior reports (e.g., Barisione et al., 2006), AAAs excised from the five mice following 28 days of continuous infusion of Ang-II tended to involve most of the suprarenal aorta and to be on the order of 2.2 mm in maximum unloaded outer diameter. In comparison, the normal unloaded outer diameter is on the order of 0.8 mm (Collins et al., 2011). Hence, Ang-II resulted in a mean 2.75-fold localized increase in diameter, consistent with the term aneurysm, which means "widening" and is generally considered pathologic if the diameter increases by 1.5 fold or more. Upon gross examination in a pilot study, however, the true lumen appeared to be preserved throughout much of the lesion, thus most of the gross dilatation resulted from an intramural accumulation of thrombus or extracellular matrix material (Figure 2). There also existed a large parallel intramural cavity (presumably a false lumen) in some regions, which merged with the true lumen in the center of the lesion to form a much larger "merged" lumen.

Also consistent with the gross observations (cf. Figure 2), serial histological sections revealed three distinctive formations in each of the five lesions (Figure 3a – c). Formation (a) consistently appeared within the region of maximum dilatation, which was typically near the center of the lesion; it was characterized by a ruptured media, that is, completely severed elastic fibers and smooth muscle at a single circumferential location within the media. This rupture allowed a large cavity, presumably a false lumen, to merge with the true lumen. This merged lumen is illustrated well in the VVG-stained cross-section shown as Figure 3a wherein the wavy elastic fibers appear black and the two arrows point to the site of medial rupture. Formation (b) typically existed close to and just distal and proximal to the site of the merged lumen; it was characterized by an intact lumen and parallel cavity that were separated by what appeared to be remodeled matrix (Figure 3b). Note that the true lumen in these regions was circumscribed by an intact media consisting of concentric elastic lamellae as expected of a normal aortic wall (cf. Collins et al., 2011). Formation (c) was found the farthest from the site of the merged lumen, again both distal and proximal, and was characterized by an intact true lumen and an intramural thrombus that typically consisted of fibrin (Figure 3c) but in some cases GAGs and fibrillar collagen (Figures 4 and 5). Again, the true lumen was circumscribed by an apparently normal media. It should be noted that black fragments visible on the outer perimeter in all cross-sections in Figure 3 are remnant India ink, which was used in mechanical tests that are reported elsewhere (Genovese et al., 2012). Furthermore, the symbols † and ‡ in Figure 3 denote locations where the waviness and concentration of fibrillar collagen were calculated, as described below.

Staining with Movat's pentachrome and PSR revealed marked spatial distributions of fibrillar collagen, fibrin, and GAGs (Figures 4 and 5). Recall, therefore, that collagen appears brownish/gray in sections stained with Movat's pentachrome while fibrin appears pink/red, GAGs light blue, and elastic fibers black. In contrast, type I, or thick, collagen

fibers appear bright red/orange whereas type III, or thin, collagen fibers appear less bright and more green/yellow in sections stained with PSR and viewed using polarized light. The large pink region in the Movat's stain in Figure 4 revealed an extensive asymmetric accumulation of fibrin, with little fibrillar collagen as confirmed by the lack of bright birefringence in the associated PSR image. Yet, at some locations near the expanding adventitia, brownish/light blue colors suggested the presence of small pockets of GAGs (e.g., white asterisk in Figure 4a) and collagen fibers (white arrows in Figure 4b), which may mark regions where the thrombus was beginning to remodel towards a collagenous tissue. Such a deposition of GAGs and fibrillar collagen may have reflected a wound healing type response, perhaps mediated by myofibroblasts consistent with the co-localized αSMA staining (Figure 4c) and known ability of this cell type to deposit significant amounts of collagen (Tomasek et al., 2002; Hinz et al., 2007). Regardless, Figure 5 shows nearly sequential sections that were located farther yet from the center of the lesion and stained with PSR (a), Movat's pentachrome (b), or Alcian blue (c), with thresholding used to highlight fibrin in the Movat's stain and GAGs in the Alcian blue stain. These sections contained more collagen (Figure 5a) and correspondingly more GAGs (Figure 5c) and less fibrin (Figure 5b) within the intramural region presumably occupied by thrombus at some time. Indeed, the collagen and GAGs tended to co-localize in regions devoid of fibrin, hence implying a replacement process.

Given that it should take some time for fibrin to break down and for synthetic cells to invade the thrombus and produce significant amounts of collagen, Figures 4 and 5 may suggest different relative "ages" for the thrombus, that is, times since that portion of the thrombus was either formed from or in contact with the flowing blood. Thus, one might speculate that the youngest thrombus existed closest to the center of the lesion where the merged lumen could have continued to provide flowing blood (formation (a), Figure 3a), and hence fibrinogen and platelets, whereas the oldest region of the same thrombus existed farthest from the merged lumen and hence the flowing blood. This possibility is supported by findings in Figure 6, which show higher magnification images (60X) of thrombus from progressively greater distances (left to right) from the patent cavity (i.e., locations separated axially by 880 microns within the same thrombus that is seen in Figure 4). Note again that the spatio-temporal decrease in fibrin (pink) corresponded with the increase in GAGs (blue) and collagen (birefringent in the darkfield image). Moreover, the sequence of picrosirius red stained images (b,d,f) revealed both an increase in collagen concentration and fiber thickness (brighter red) with remodeling, or aging, of the thrombus. The "holes" in the birefrigent images likely corresponded to locations of synthetic cells, although possibly caniculi (cf. Wang et al., 2001).

During our examinations of sections stained with PSR, we also noticed changes in collagen organization and appearance within the adventitia when comparing regions close to the true lumen (e.g., denoted by † in Figure 3) with those well away from the lumen (e.g., denoted by ‡ in Figure 3). Because of the tremendous asymmetric increase in diameter, collagen well away from the lumen must necessarily have remodeled (that is, collagen can only extend on the order of 10% once straight, yet some portions of the adventitia farthest from the lumen must have elongated on the order of 150 to 200% during the 28-day period of study). Figure 7 shows two dark-field images that highlight representative differences in collagen organization between locations † and ‡. Quantified differences in collagen waviness and concentration, relative to near normal values, are shown in Figure 8 at these two locations for all three formations (a: merged lumen, b: lumen plus cavity, c: lumen plus intramural thrombus in Figure 3). Specifically, comparisons between locations ‡ and † in the adventitia are given by dark gray bars for the three formations in Figure 3 (i.e., $a - c_1$ here). In contrast, comparisons between collagen within a remodeled intramural thrombus and adventitial location † are given by the light gray bars (bar c_2). Zero denotes a waviness or concentration

equivalent to that in the adventitia nearest the lumen (location †), which was assumed to be the closest to normal within this cross-section. This analysis suggested that the remodeled collagen fibers at location ‡ were always less wavy than the more normal collagen fibers at location †, which is reflected by the decrease in entropy (formations a – c_1). Conversely, remodeled collagen fibers within the intramural thrombus were significantly more disorganized / wavy than normal as reflected by the increased entropy (bar c_2). No significant differences were found in collagen waviness amongst the three thrombi shown in Figure 6, however (i.e., the picrosirius stained images in panels (b), (d), and (f)). These objective quantitative findings were expected based on visual assessments, as, for example, when comparing collagen organization in Figure 7a (more normal adventitia) with Figures 6ba, 6d, and 6f (remodeled intramural thrombus).

Results for the concentration of collagen (Figure 8b) revealed a significant decrease in the remodeled adventitia compared to the normal adventitia (formations a – c_1). This finding was also consistent with our visual impression from images such as that in Figure 7, wherein collagen appeared more densely packed at location † compared with location ‡. The lowest concentration of collagen fibers was found in the remodeled intramural thrombus, bar c_2, but the specific value of the concentration depended on both the location within the thrombus and the remodeling time. For example, the mean relative difference (relative to near normal collagen; cf. Figure 7a) and corresponding standard errors of the mean for collagen concentration of the young, older, and oldest thrombus were −56.8 +/− 6.2%, −31.7 +/− 2.6%, and 14.1 +/− 0.9%, respectively. This progressive increase in collagen concentration appeared to be consistent with an increasing thrombus age / remodeling time (cf. Figure 6).

DISCUSSION

Angiotensin-II is a potent vasopressor having pleiotropic activity. For example, systemic increases of Ang-II in the bloodstream can cause vasoconstriction throughout the arterial tree, and thus increased systemic blood pressure; conversely, local increases of Ang-II within the arterial wall can lead to the increased production of diverse chemokines, cytokines, and proteases, which can cause significant localized remodeling of the wall. Although hypertension is a risk factor for human aortic aneurysms and dissections, Cassis et al. (2009) showed that Ang-II results in dissecting suprarenal aortic aneurysms in mice independent of blood pressure. Rather, it appears to be the macrophages and other inflammatory cells that are recruited to the media and adventitia of the suprarenal aorta that play key roles in the initiation and development of these AAAs (Tieu et al., 2009) while other large arteries are spared (Bersi et al., 2012). Indeed, this concept of a localized macrophage mediated pathogenesis is consistent with the stimulation of monocyte chemoattractant protein 1 by Ang-II (Mehta and Griendling, 2007), which facilitates the recruitment of monocytes / macrophages to the aortic wall.

Although aortic lesions resulting from subcutaneous infusion of Ang-II in the mouse are typically suggested to model certain aspects of abdominal aortic aneurysms, AAAs seldom dissect in humans. In contrast, the present findings are consistent with the early report by Saraff et al. (2003) that Ang-II induced aneurysms in the mouse arise following an aortic dissection. For this reason, this animal model may be a better model of some aspects of TAAs, which often dissect and are similarly not well understood biomechanically (Milewicz et al., 2008; Grond-Ginsbach et al., 2011). Nevertheless, a detailed study of histological and mechanical characteristics of this mouse model will increase our general understanding of the initiation and propagation of dissecting arteries and aneurysms. Towards this end, of course, there is a need for additional longitudinal data, particularly at early time points when the lesion initiates.

Consistent with prior reports (cf. Daugherty et al., 2011), we found that the dissection at 28 days presented as three prototypically different formations along the axial direction (cf. Figures 2 and 3): a central region wherein medial elastic lamellae fragmented completely and the true lumen merged with a false lumen; regions distal and proximal to the central region wherein the media remained intact but there existed a large intramural cavity (false lumen) without thrombus; and regions more distal and proximal to the central region wherein the media remained intact but the intramural cavity was filled with either thrombus or remodeled thrombus consisting largely of GAGs and collagen. Little prior attention has been directed toward the potential remodeling of the intramural thrombus. Note, therefore, that clinical observations in patients having a dissecting TAA suggest that a patent false lumen may be a potential risk factor for continued aortic enlargement and a poor long-term outcome, but a partially thrombosed false lumen may be of even greater concern (Clough et al., 2011; Bode-Janisch et al., 2012), perhaps due to increased plasmin activity (cf. Deng et al., 2003) since plasmin can activate latent matrix metalloproteinases (Lijnen, 2001). In contrast, a fully thrombosed false lumen may be protective, serving as a first step in “aortic wall healing and remodeling after repair” (Song et al., 2011). The present observations support the hypothesis that a thrombus isolated from flowing blood may allow invading cells to replace the degrading fibrin with fibrillar collagens (cf. Irniger, 1963; Fineschi et al., 2009; Karsaj and Humphrey, 2010), which could potentially strengthen the wall and protect it from possible further dissection or rupture, at least within that region. Indeed, this hypothesis is consistent with the tacit assumption underlying the treatment of intracranial saccular aneurysms with clot-promoting coils or flow-diverting stents. In this case, it is hoped that an intra-saccular thrombosis will form and become isolated from the bloodstream (e.g., via re-endothelialization at the orifice of the lesion), thus allowing subsequent conversion of the thrombus to collagenous tissue by invading myofibroblasts (Lee et al., 2007). What appears to be vital, therefore, is that the intramural or intraluminal clot be isolated from flowing blood, which of course can otherwise serve as a replenishing source of platelets, leukocytes, fibrinogen (and thus fibrin), plasminogen (and thus plasmin), and so forth.

Whereas an endograft can isolate an intraluminal thrombus within an AAA from the flowing blood, such a thrombus remains in contact with the bloodstream under “normal” conditions. In contrast, much of the intramural thrombus within the false lumen of a dissected artery or aneurysm could naturally become isolated from the flowing blood even if the “ends” of the thrombus are never so isolated. In this case, as in the case of the coiled intracranial aneurysm (cf. Lee et al., 2007), it is possible that cells having synthetic capability can invade and remodel the thrombus provided that there is sufficient oxygenation and modest levels of competing cells and biomolecules that arise from the blood – thrombus interface (cf. Houard et al., 2007; Folkesson et al., 2011). Our findings support this possibility. Recall, too, that we found αSMA-positive cells within both the media, where smooth muscle cells are to be expected, and co-localized with regions experiencing new collagen and GAG deposition (cf. Figure 4). It is well known that myofibroblasts exhibit heightened synthetic capability, that they are fundamental to connective tissue remodeling in many tissues and organs, and that αSMA is the most commonly used marker for this cell type (Tomasek et al., 2002). Moreover, there now appears to be many possible sources of myofibroblasts, including adventitial fibroblasts and resident progenitor cells, bone marrow derived fibrocytes, smooth muscle cells, and even (via endothelial-to-mesenchymal transistions) endothelial cells (Hinz et al., 2007). Although we neither attempted to confirm that the αSMA-positive cells were indeed myofibroblasts nor tried to identify cell source, our observations were consistent with a radially inward invasion of myofibroblasts from the adventitia into the thrombus (cf. Figure 4), similar to that reported by Lee et al. (2007) in a very different model of remodeling of thrombus via collagen deposition. This complex issue clearly merits further

study, however, particularly given the increasing interest in adventitial cells in vascular remodeling (Maiellaro and Taylor, 2007).

The present findings also do not provide any further information on possible reasons why a partially thrombosed dissection may be more susceptible to further dissection or rupture. There was no indication of local adverse remodeling or failure of the wall / remnant adventitia in regions containing fibrin-rich thrombus (e.g., Supplemental Figure 2). Indeed, it appears that if the aortic wall ruptures in this mouse model, it tends to do so early in the development of the dissection (generally 4–10 days following the initiation of Ang-II infusion; Barisone et al., 2006), perhaps during the period when all or most of the thrombus is newly formed. We focused herein on later development, 28 days following the initiation of Ang-II, to capture different stages of thrombus development within single lesions. There is a need nonetheless to explore earlier time points further, particularly given the observation by Saraff et al. (2003) that “Macrophage accumulation was particularly evident at the edges of the thrombi, both in regions of disrupted and intact media.” There is similarly motivation to quantify possible temporal changes in blood-borne biomarkers or factors involved in the clotting process.

Finally, we suggest one possible scenario (Figure 9) that is consistent with our histological observations, that is, the existence of three distinct formations (cf. Figures 2 and 3) in each of our five vessels and the different stages of thrombus remodeling therein. Figure 9a shows the possible initiation of an intramural delamination (due, in part, to the medial accumulation of macrophages; Daugherty et al., 2011), followed by a possible propagation of this delamination in Figure 9b (due to wall stresses exceeding local inter-lamellar strength) that ultimately leads to dissection along the medial – adventitial border and a subsequent localized transmural tear that establishes communication with the lumen. Intramural pressures caused by the blood could then contribute to the propagation of a dissection and initiate associated growth and remodeling processes within the remaining intramural constituents (Tiessen and Roach, 1993), leading to the observed dramatic increase in vessel circumference and formation of an intramural thrombus. Regardless of the specific mechanisms responsible for the pathogenesis, Figure 9c illustrates a longitudinal section as a possible scenario for an advanced, 28-day dissecting aneurysm (cf. Figure 3 in Cao et al., 2010). Panels 9d – f show how the longitudinal section of Figure 9c might appear in typical histological cross-sections, which match the three formations we observed in all five lesions (cf. Figures 2 and 3). Additionally, relative differences in the age of the thrombus (i.e., time since it was in contact with flowing blood) can be explained using this scenario. The youngest region of the thrombus would occur near the center of the aneurysm, where it is exposed to the blood stream via the ruptured intimal-medial layer. The oldest regions of thrombus would be farthest from the center of the lesion and not directly exposed to blood; this would allow more time, and perhaps a more permissive environment, for synthetic cells to invade the intramural thrombus and to start the remodeling process (cf. Figures 4 and 6).

In summary, we have presented new observations related to collagen remodeling within dissecting aneurysms that arise in the most commonly employed mouse model of aortic aneurysms. The rapidly expanding adventitia clearly undergoes remarkable remodeling, but so too the intramural thrombus in regions well separated from the flowing blood. Given that replacement of thrombus by collagenous tissue may represent a favorable wound healing response, additional effort should be directed toward understanding and promoting such remodeling in arterial dissections. Insight gained could also have a broader impact, as, for example, in providing new insight relative to the use of endografts (and so-called endoleak) to treat aortic aneurysms or flow-diverting stents to treat intracranial aneurysms.

Acknowledgments

This work was supported, in part, by generous contributions to Texas A&M University by Tommie E. and Carolyn S. Lohman, grants from the NIH (R01 HL086418) and the European Commission FP7 SCATh (#248782), and a Marshall Plan Scholarship that supported A. Schriefl as a Visiting Assistant in Research at Yale University. We also thank Dr. E. Wilson at the Texas A&M Health Science Center for maintaining the ApoE−/− colony and Dr. Y.U. Lee and Mr. J. Ferruzzi at Yale University for overseeing the initial histological preparation of the samples.

References

Barisione C, Charnigo R, Howatt DA, Moorleghen JJ, Rateri DL, Daugherty A. Rapid dilatation of the abdominal aorta during infusion of angiotensin II detected by noninvasive high-frequency ultrasonography. J Vasc Surg. 2006; 44:372–376. [PubMed: 16890871]

Bayan C, Levitt JM, Miller E, Kaplan D, Georgakoudi I. Fully automated, quantitative, noninvasive assessment of collagen fiber content and organization in thick collagen gels. J Appl Phys. 2009; 105:102042.

Bersi MR, Collins MJ, Wilson E, Humphrey JD. Disparate changes in the mechanical properties of murine carotid arteries and aorta in response to chronic infusion of angiotensin-II. Int J Adv Eng Sci Appl Math. 2012 (in press).

Bode-Jänisch S, Schmidt A, Günther D, Stuhrmann M, Fieguth A. Aortic dissecting aneurysms – Histopathological findings. Forensic Sci Int. 2012; 214:13–17. [PubMed: 21794994]

Cao RY, Amand TS, Ford MD, Piomelli U, Funk CD. The murine angiotensin II-induced abdominal aortic aneurysm model: rupture risk and inflammatory progression patterns. Front Pharmacol. 2010; 1:9. [PubMed: 21713101]

Cassis LA, Gupte M, Thayer S, Zhang X, Charnigo R, Howatt DA, Rateri DL, Daugherty A. ANG II infusion promotes abdominal aortic aneurysms independent of increased blood pressure in hypercholesterolemic mice. Am J Physiol Heart Circ Physiol. 2009; 296:H1660–1665. [PubMed: 19252100]

Clough RE, Hussain T, Uribe S, Greil GF, Razavi R, Taylor PR, Schaeffter T, Waltham M. A new method for quantification of false lumen thrombosis in aortic dissection using magnetic resonance imaging and a blood pool contrast agent. J Vasc Surg. 2011; 54:1251–1258. [PubMed: 21906904]

Collins MJ, Bersi M, Wilson E, Humphrey JD. Mechanical properties of suprarenal and infrarenal abdominal aorta: implications for mouse models of aneurysms. Med Eng Phys. 2011; 33:1262–1269. [PubMed: 21742539]

Daugherty A, Cassis LA. Mouse models of abdominal aortic aneurysms. Arterioscler Thromb Vasc Biol. 2004; 24:429–434. [PubMed: 14739119]

Daugherty A, Cassis LA, Lu H. Complex pathologies of angiotensin II-induced abdominal aortic aneurysms. J Zhejiang Univ-Sci B. 2011; 12:624–628. [PubMed: 21796801]

Deng GG, Martin-McNulty B, Sukovich DA, Freay A, Halks-Miller M, Thinnes T, Loskutoff DJ, Carmeliet P, Dole WP, Wang Y-X. Urokinase-type plasminogen activator plays a critical role in angiotensin II-induced abdominal aortic aneurysm. Circ Res. 2003; 92:510–517. [PubMed: 12600880]

Fineschi V, Turillazzi E, Neri M, Pomara C, Riezzo I. Histological age determination of venous thrombosis: a neglected forensic task in fatal pulmonary thrombo-embolism. Forensic Sci Int. 2009; 186:22–28. [PubMed: 19203853]

Folkesson M, Silveira A, Eriksson P, Swedenborg J. Protease activity in the multi-layered intra-luminal thrombus of abdominal aortic aneurysms. Atherosclerosis. 2011; 218:294–299. [PubMed: 21632052]

Genovese K, Collins MJ, Lee YU, Humphrey JD. Regional finite strains in an angiotensin II induced mouse model of dissecting abdominal aortic aneurysms. Cardiovasc Engr Tech. 2012 (in press).

Goergen CJ, Azuma J, Barr KN, Magdefessel L, Kallop DY, Gogineni A, Grewall A, Weimer RM, Connolly AJ, Dalman RL, Taylor CA, Tsao PS, Greve JM. Influences of aortic motion and curvature on vessel expansion in murine experimental aneurysms. Arterioscler Thromb Vasc Biol. 2011; 31:270–279. [PubMed: 21071686]

Grond-Ginsbach C, Pjontek R, Aksay SS, Hyhlik-Durr A, Bockler D, Gross-Weissmann ML. Spontaneous arterial dissection: phenotype and molecular pathogenesis. Cell Molc Life Sci. 2010; 67:17990–1815.

Hinz B, Phan SH, Thannickal VJ, Galli A, Bochaton-Pillat ML, Gabbiani G. The myofibroblast: one function, multiple origins. Am J Path. 2007; 170:1807–1816. [PubMed: 17525249]

Houard X, Rouzet F, Touat Z, Philippe M, Dominguez M, Fontaine V, Sarda-Mantel L, Meulemans A, Le Guludec D, Meilhac O, Michel J-B. Topology of the fibrinolytic system within the mural thrombus of human abdominal aortic aneurysms. J Pathol. 2007; 212:20–28. [PubMed: 17352452]

Humphrey, JD. Cardiovascular Solid Mechanics: Cells, Tissues, and Organs. Springer; NY: 2002.

Humphrey JD, Taylor CA. Intracranial and abdominal aortic aneurysms: Similarities, differences, and need for a new class of computational models. Ann Rev Biomed Engr. 2008; 10:221–246.

Humphrey JD, Holzapfel GA. Mechanics, mechanobiology, and modeling of human abdominal aorta and aneurysms. J Biomech. 2012; 45:805–814. [PubMed: 22189249]

Irniger W. Histologische Altersbestimmung von Thrombosen und Embolien. Virchows Arch path Anat. 1963; 336:220–237.

Karšaj I, Humphrey JD. A mathematical model of the evolving mechanical properties of intraluminal thrombus. Biorheology. 2010; 46:509–527.

Lee D, Yuki I, Murayama Y, Chiang A, Nishimura I, Vinters HV, Wang CJ, Nien Y-L, Ishii A, Wu BM, Viñuela F. Thrombus organization and healing in the swine experimental aneurysm model. Part I. A histological and molecular analysis. J Neurosurg. 2007; 107:94–108. [PubMed: 17639879]

Lijnen HR. Plasmin and matrix metalloproteinases in vascular remodeling. Thromb Haemost. 2001; 86:324–333. [PubMed: 11487021]

Luo J, Fujikura K, Tyrie LS, Tilson MD, Konofagou EE. Pulse wave imaging of normal and aneurysmal abdominal aortas in vivo. IEEE Trans Med Imaging. 2009; 28:477–486. [PubMed: 19272985]

Maiellaro K, Taylor WR. The role of the adventitia in vascular inflammation. Cardiovasc Res. 2007; 75:640–648. [PubMed: 17662969]

Mehta PK, Griendling KK. Angiotensin-II cell signaling: physiological and pathological effects in the cardiovascular system. Am J Physiol. 2007; 292:C82–97.

Milewicz DM, Guo DC, Tran-Fadulu V, Lafont AL, Papke CL, Inamoto S, Kwartler CS, Pannu H. Genetic basis of thoracic aortic aneurysms and dissections: focus on smooth muscle cell contractile dysfunction. Annu Rev Genomics Human Genet. 2008; 9:283–302. [PubMed: 18544034]

Rateri DL, Howatt DA, Moorleghen JJ, Charnigo R, Cassis LA, Daugherty A. Prolonged infusion of angiotensin II in apoE −/− mice promotes macrophage recruitment with continued expansion of abdominal aortic aneurysm. Am J Pathol. 2011; 179:1542–1548. [PubMed: 21763672]

Rush C, Nyara M, Moxon JV, Trollope A, Cullen B, Golledge J. Whole genome expression analysis within the angiotensin II – apolipoprotein E deficient mouse model of abdominal aortic aneurysm. BMC Genomics. 2009; 10:298. [PubMed: 19580648]

Sakalihasan N, Limet R, Defawe OD. Abdominal aortic aneurysm. Lancet. 2005; 365:1577–1589. [PubMed: 15866312]

Saraff K, Babamusta F, Cassis LA, Daugherty A. Aortic dissection precedes formation of aneurysms and atherosclerosis in angiotensin-II infused, apolipoprotein E-deficient mice. Arterioscl Thromb Vasc Biol. 2003; 23:1621–1626. [PubMed: 12855482]

Satoh K, Nigro P, Matoba T, O'Dell MR, Cui Z, Shi X, Mohan A, Yan C, Abe J-I, Illig KA, Berk BC. Cyclophilin A enhances vascular oxidative stress and the development of angiotensin-II induced aneurysms. Nat Med. 2009; 15:649–656. [PubMed: 19430489]

Song S-W, Yoo K-J, Kim D-K, Cho B-K, Yi G, Chang B-C. Effects of early anticoagulation on the degree of thrombosis after repair of acute DeBakey type I aortic dissection. Ann Thorac Surg. 2011; 92:1367–1375. [PubMed: 21864829]

Tiessen IM, Roach MR. Factors in the initiation and propagation of aortic dissections in human autopsy aortas. J Biomech Engr. 1993; 115:123–124.

Tieu BC, Lee C, Sun H, LeJeune W, Recinos A 3rd, Ju X, Spratt H, Guo DC, Milewicz D, Tilton RG, Brasier AR. An adventitial IL-6/MCP-1 amplification loop accelerates macrophage-mediated vascular inflammation leading to aortic dissection in mice. J Clin Invest. 2009; 119:3637–3651. [PubMed: 19920349]

Tomasek JJ, Gabbiani G, Hinz B, Chaponnier C, Brown RA. Myofibroblasts and mechano-regulation of connective tissue remodeling. Nat Rev Molc Cell Biol. 2002; 3:349–363.

Trachet B, Renard M, De Santis G, Staelens S, De Backer J, Antiga L, Loeys B, Segers P. An integrated framework to quantitatively link mouse-specific hemodynamics to aneurysm formation in angiotensin II-infused ApoE −/− mice. Ann Biomed Eng. 2011; 39:2430–2444. [PubMed: 21614649]

Vorp DA. Biomechanics of abdominal aortic aneurysm. J Biomech. 2007; 40:1887–1902. [PubMed: 17254589]

Wang DHJ, Makaroun MS, Webster MW, Vorp DA. Effect of intraluminal thrombus on wall stress in patient-specific models of abdominal aortic aneurysm. J Vasc Surg. 2002; 36:598–604. [PubMed: 12218961]

Xia Y, Elder K. Quantification of the graphical details of collagen fibrils in transmission electron micrographs. J Microsc. 2001; 204:3–16. [PubMed: 11580808]

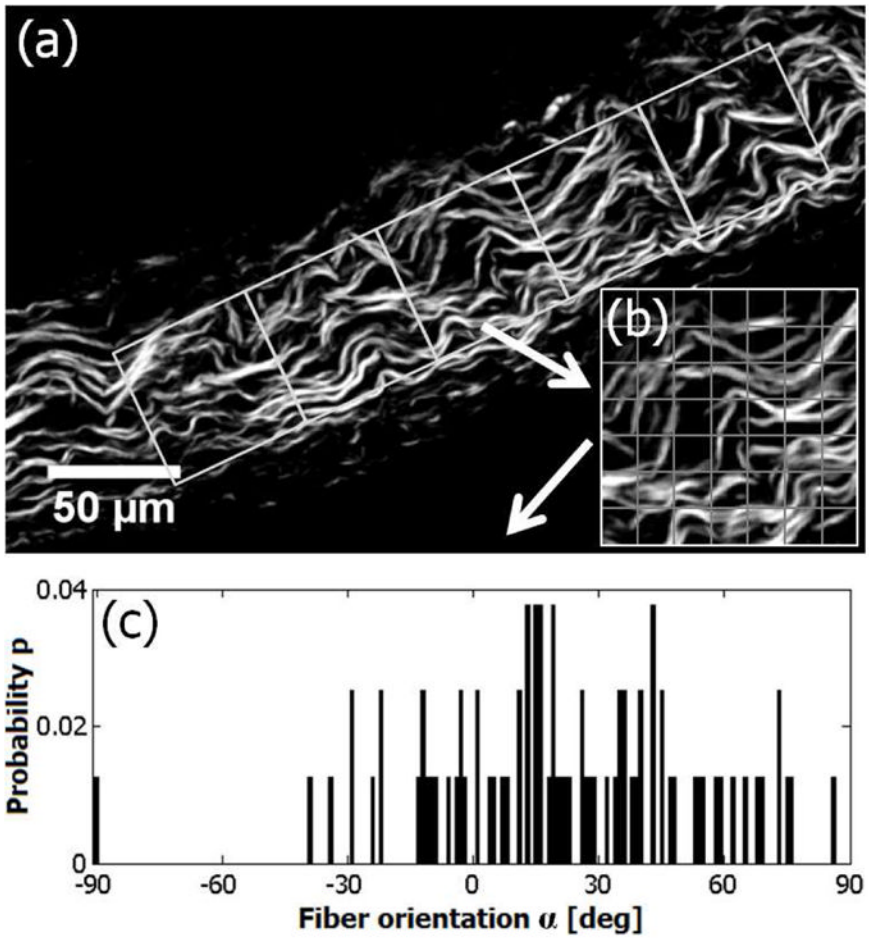

Figure 1.

Schematic of steps to compute entropy H as a measure of collagen waviness or disorder. (a) An original dark-field image of a portion of the PSR-stained adventitia is shown with five associated subdomains defined for separate computations. (b) Each sub-domain was divided into $m \times m$ pixel regions of interest (ROIs) as shown by the light grid lines in this representative sample. (c) The overall fiber orientation α was determined for each ROI and plotted as a normalized histogram to yield the probability mass function p as defined in the text.

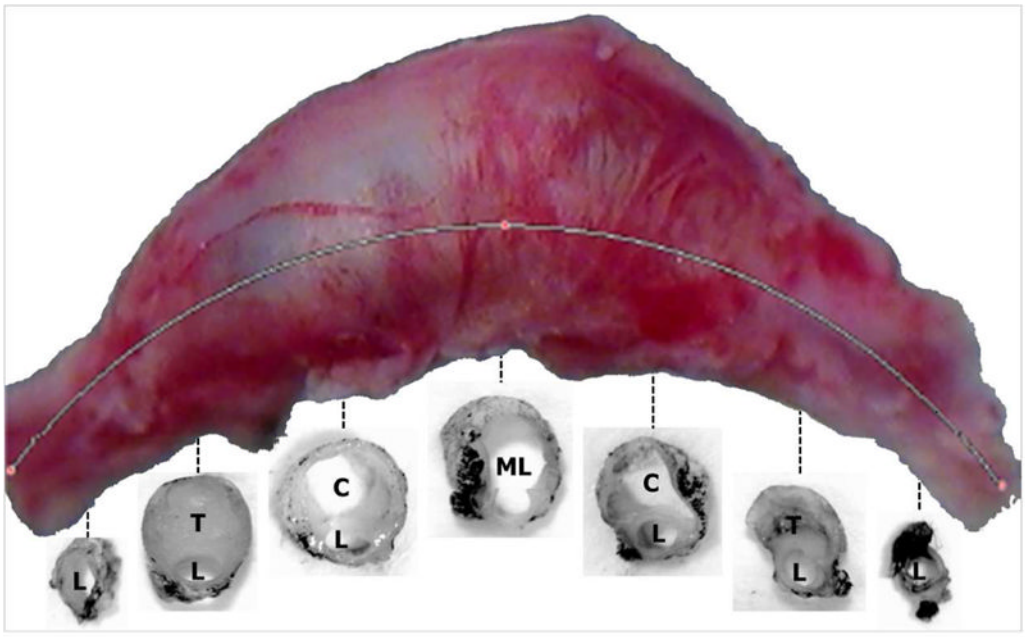

Figure 2.

Photograph of a representative suprarenal aortic aneurysm that resulted following 28 days of a subcutaneous infusion of Ang-II in the ApoE−/− mouse; the maximum diameter is ~2.2 mm. Shown, too, are reduced magnification photographs of cross-sections obtained from regions indicated by the dashed lines: **L** – lumen, **T** – thrombus, **C** – cavity, and **ML** – merged lumen (i.e., probable merging of the true lumen **L** with a false lumen / cavity). As noted in the text, the thrombus contained different constituents depending on its position within the lesion as well as its distance from the region of maximal dilatation. Note that the black in the photographs of the cross-sections is India ink from a prior mechanical test.

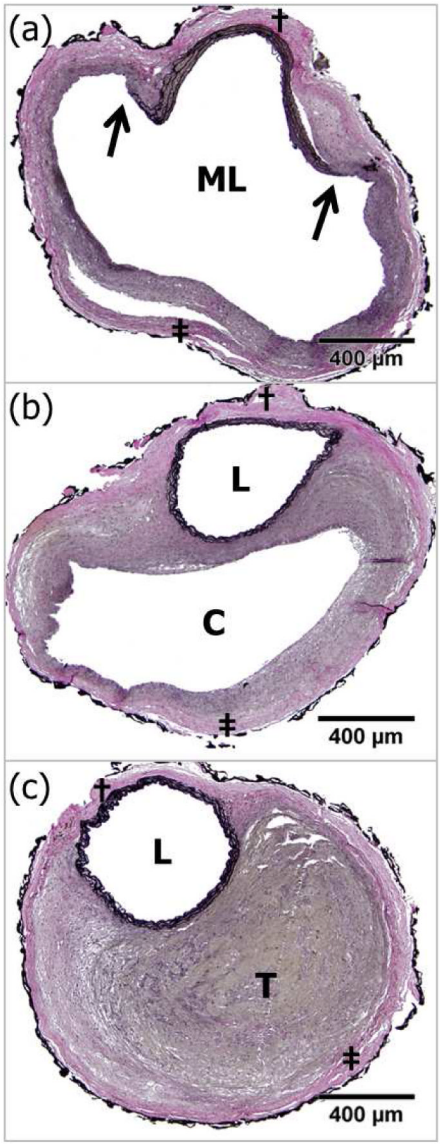

Figure 3.

Representative Verhoeff Van Gieson (VVG)-stained cross-sections that reveal the three distinct formations that were observed in each of the five dissecting aneurysms studied. Note: the wavy elastic fibers within the aortic media appeared black; in contrast, the black fragments along the outermost perimeter are due to India ink that was used in mechanical tests that are reported elsewhere. Formation (a): merged lumen (ML), with arrows indicating locations where the media ruptured, thus allowing the true lumen and outer cavity (false lumen) to communicate. Formation (b): intact lumen (L) and cavity (C) separated by remodeled tissue; this cavity is presumably a false lumen. Formation (c): intact lumen (L) and intramural thrombus (T). The symbols † and ‡ denote locations used for subsequent analysis of the waviness and concentration of fibrillar collagen.

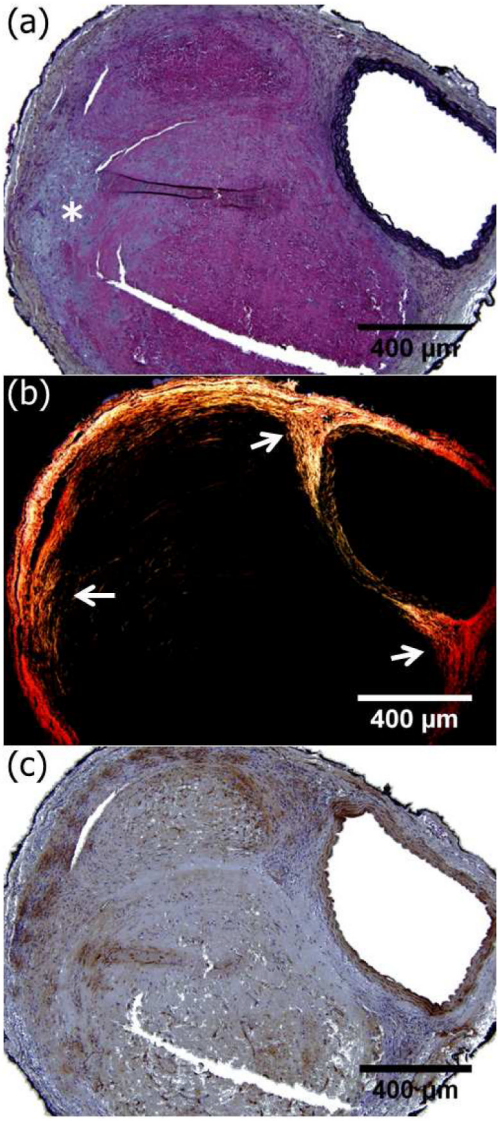

Figure 4.

Movat's Pentachrome (a), dark-field picrosirius red (b), and alpha-smooth muscle (c) stained images of nearby aneurysmal cross-sections. Note that the Movat's stain shows elastic fibers as black, fibrin as pink/red, GAGs as light blue, and collagen as brownish/gray; the darkfield picrosirius stain shows collagen type I or thicker fibers as bright red/orange and collagen type III or thinner fibers as less bright and more green/yellow; the alpha smooth muscle strain shows both smooth muscle cells and myofibroblasts as brown. Hence, pink regions in (a) reveal thrombotic material (fibrin) that had not remodeled, which was confirmed by the lack of fibrillar collagen in the associated regions within (b). In contrast, regions wherein the pink was replaced by brownish / light blue colors in (a) indicated regions wherein the fibrin may have started to remodel, presumably via the deposition of GAGs (white asterisk in a) and fibrillar collagen (e.g., horizontal white arrow in b) by co-localized invading αSMA-positive cells, which may well have been myofibroblasts.

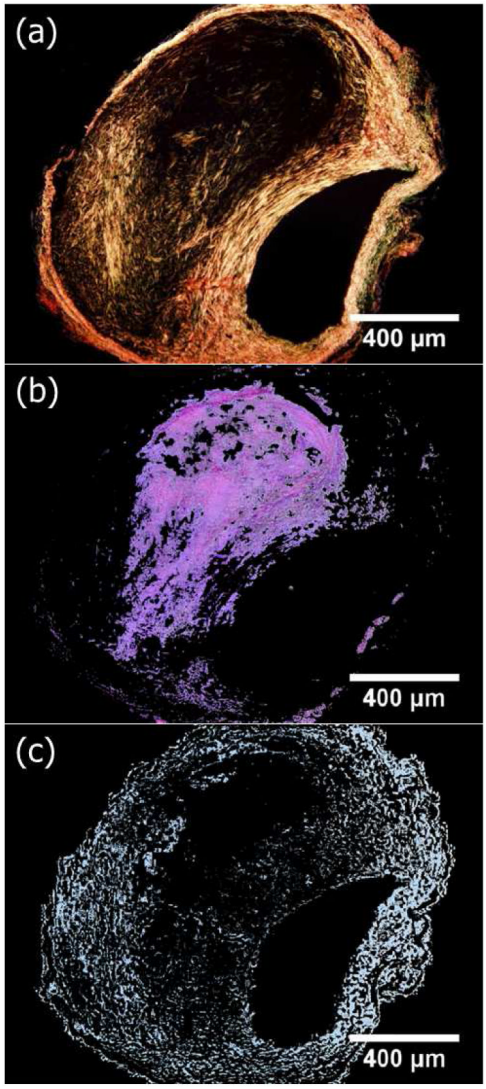

Figure 5.

Representative images from nearby cross-sections that were located distant from the center of the lesion. Isolated constituents were highlighted by polarizing light or thresholding: (a) dark-field polarized light image of a picrosirius-stained section showing fibrillar collagen, (b) thresholded image of pink thrombus revealed by a Movat's Pentachrome stained section, and (c) thresholded image of a bluish deposition of glycosaminoglycans (GAGs) revealed by a separate Alcian blue stained section. Notice the lack of collagen in areas of fibrin-rich thrombus, but the colocalization of fibrillar collagen and GAGs in the remodeled regions. Note: The single constituents in panels b and c were extracted from the original images using color thresholding in ImageJ.

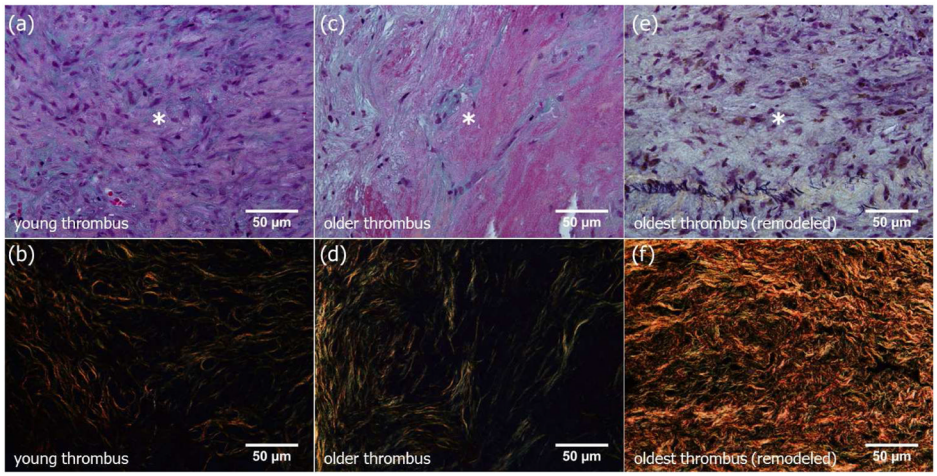

Figure 6.

Close-up (60X) images of three regions of intramural thrombus stained with either Movat's Pentachrome (top panels) or picrosirius red (bottom panels). Panels (a) and (b) show thrombus that was closest to the center of the lesion, which likely represented the "youngest" thrombus, that is, replenished due to its proximity to the flowing blood. Panels (c) and (d) are from the same lesion but ~880 microns farther from the center, and thus likely represent a slightly older thrombus. Panels (e) and (f) are from a region ~1760 microns away from the center of the lesion, and thus likely farthest from the free flowing blood and thereby the oldest. The series of the picrosirius-stained images (b,d,f) highlights changes in collagen structure and organization from that originally laid down around cells or canaliculi (circular structures) in the youngest (or biologically most active) thrombus (b), to more fibrillar collagen structures in (d), and finally to highly remodeled thrombus in (f). The increase in collagen concentration was consistent with the decrease of fibrin, which appeared pink/red in the Movat's stain. Recall that this dramatic remodeling took place within about three weeks.

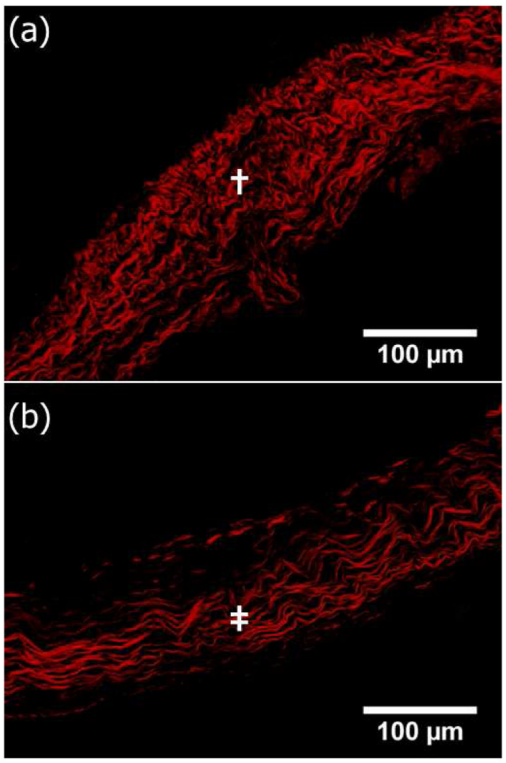

Figure 7.
Representative dark-field images of sections stained with picrosirius red to highlight collagen fibers in the adventitia at location † (presumed nearly normal adventitia just behind the lumen) and location ‡ (clearly remodeled collagen, well opposite the site of †). Both locations are defined in Figure 3.

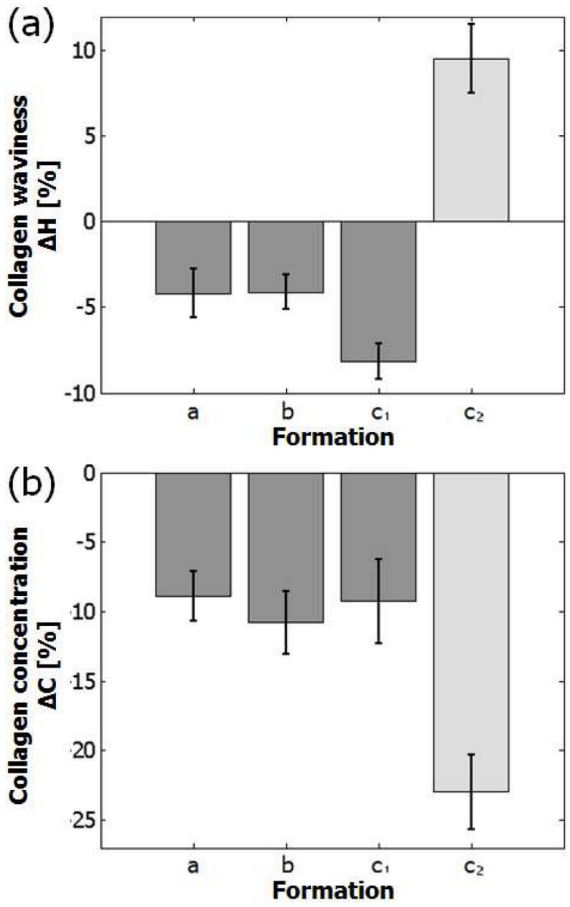

Figure 8.

Mean relative differences (relative to near normal collagen; cf. Figure 6b) and corresponding standard errors of the mean (SEM) for (a) collagen waviness and (b) collagen concentration for the three distinct cross-sectional formations present within the dissecting aneurysms. Formation (a) from Figure 3 with a merged lumen (ML); formation (b) from Figure 3 with an isolated lumen and cavity (L and C); formations c_1 and c_2 from Figure 3 with a lumen and intramural thrombus (L and T) for regions that were either not remodeled (c_1) or remodeled (c_2) as indicated by collagen deposition. The dark gray bars (formations a – c_1) denote comparisons between locations ‡ and † in adventitial regions. The light gray bars (formation c_2) denote comparisons between collagen in a remodeled intramural thrombus (T) and adventitial collagen at location †. Zero thus denotes the waviness and concentration of collagen within the nearly normal adventitia behind the lumen (location †). All formations and locations are defined in Figure 3.

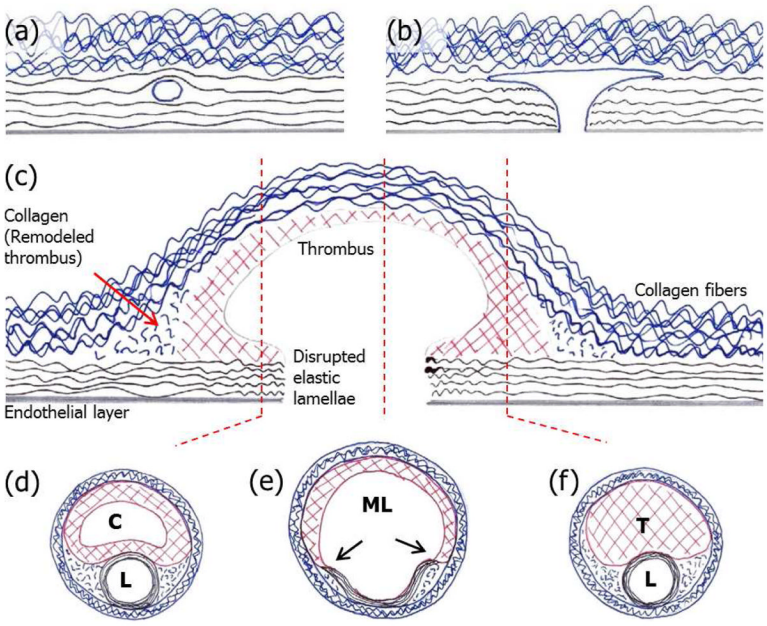

Figure 9.

A postulated (a) intramural initiation of a localized delamination within the media of the suprarenal aorta in an ApoE−/− mouse infused with angiotension-II that (b) could propagate and lead to both a dissection along the medial-adventitial plane and an intimal-medial tear, with subsequent communication with the blood stream that could allow a false lumen to extend axially (c). Moreover, consistent with Figures 2 and 3, panels d – f show types of cross-sections that could arise due to the false lumen filling with thrombus on the more distal and proximal aspects, with those regions farthest from the flowing blood experiencing a replacement of fibrin with newly deposited fibrillar collagen (and GAGs). It is possible, of course, that the initial dissection could propagate within the media (not found in this study), along the medial-adventitial border, or within the adventitia, particularly if it had previously remodeled into more loosely organized collagen fibers (as often observed herein).